Photoluminescence studies of Sm^{2+} in the stimulable phosphor SrS:Eu,Sm

Lawrence H. Robins
National Institute of Standards and Technology, Gaithersburg, Maryland 20899

J. Ari Tuchman
Optex Communications Corporation, Rockville, Maryland 20850

(Received 6 June 1997; revised manuscript received 12 January 1998)

The doubly rare-earth doped phosphor SrS:Eu,Sm is representative of a class of stimulable phosphors that may find application in optical data storage and related areas of photonic technology. The infrared photoluminescence (PL) from the Sm^{2+} ions is a potentially useful probe of the ''written'' state of this phosphor, i.e., the right-hand side of the charge-transfer reaction ($Eu^{2+}+Sm^{3+}\rightleftarrows Eu^{3+}+Sm^{2+}$). In the present study, several properties of the Sm^{2+} PL from bulk ceramic SrS:Eu,Sm were examined, including the emission spectrum, temperature dependence from 14 to 300 K, electron-phonon coupling, excitation spectrum, and excitation intensity dependence. The full width at half maximum of the PL emission spectrum, $W(T)$, was found to increase with temperature in a manner consistent with a linear electron-phonon coupling model, $W(T)=W_0[\tanh(\Omega/(2k_BT))]^{-1/2}$, with $W_0=0.190$ eV and coupled phonon energy $\Omega=0.026$ eV. Periodic oscillations in the PL spectrum at $T<60$ K provide direct evidence for coupling to two phonon modes, with phonon energies $\Omega_1=0.0155$ eV and $\Omega_2=0.028$ eV. The peak of the emission spectrum occurs at 0.709 eV at 14 K and increases with temperature at a rate 1.9×10^{-4} eV/K. The electron-phonon coupling model predicts that the corresponding optical absorption peak, which is anti-Stokes shifted relative to the PL peak, should occur at 1.17 eV at low temperature, or 1.23 eV at room temperature. Previous measurements of the charge-transfer excitation spectrum in SrS:Eu,Sm showed a peak at 1.25 eV, in good agreement with the model prediction. The PL excitation spectrum from 1.7 to 6.2 eV was measured at $T=14$ K. Excitation peaks were observed at 2.08 eV, ascribed to absorption to a higher excited Sm^{2+} state; at 2.65 eV, ascribed to Eu^{2+} absorption followed by Eu→Sm charge transfer; at 2.92 eV; and at 4.49 eV, ascribed to interband excitation of the SrS. [S0163-1829(98)03819-3]

I. INTRODUCTION

The stimulable phosphor system XS:Eu,Sm, where X is an alkaline-earth element (X=Mg,Ca,Sr,Ba), is a prototype for a class of phosphor materials that may find application in optical data storage applications[1] such as compact disk systems and digital photography, based on their optical memory properties. The mechanism for optical memory in a stimulable phosphor is as follows. Initially, irradiation by light within a specific wavelength range stimulates the transfer of electrons from one type of impurity, which will be called the activator, to another type of impurity, which will be called the trap. The electron transfer from the activator to the trap is called the ''write'' process and the corresponding wavelength range is called the ''write'' band. Then, after some storage time, irradiation by light within another wavelength range stimulates the reverse electron transfer process, from the traps to the activators. This reverse electron transfer is called the ''read'' process and the corresponding wavelength range is called the ''read'' band. At the conclusion of the ''read'' process, electrons may undergo radiative recombination at the activator, resulting in photoluminescence (PL) emission from the material, which allows detection of the ''read'' process.

In the XS:Eu,Sm system, Eu is the activator and Sm is the trap.[2,3] The ''write'' process comprises ionization of a Eu center ($Eu^{2+}\rightarrow Eu^{3+}+e^-$), followed by electron capture at a Sm center ($Sm^{3+}+e^-\rightarrow Sm^{2+}$). The ''read'' process comprises the reverse steps, ionization of a Sm center ($Sm^{2+}\rightarrow Sm^{3+}+e^-$) followed by electron capture at a Eu center ($Eu^{3+}+e^-\rightarrow Eu^{2+}$). The overall charge transfer reaction, written ($Eu^{2+}+Sm^{3+}\rightleftarrows Eu^{3+}+Sm^{2+}$), is driven to the right by optical excitation in the ''write'' band and to the left by optical excitation in the ''read'' band. If the electron captured by the Eu center in the ''read'' process undergoes radiative recombination from a $(5d)$ excited state, $Eu^{2+}(4f^6 5d)$, to the $(4f)$ ground state, $Eu^{2+}(4f^7)$, then PL is emitted. The SrS:$Eu^{2+}(5d\rightarrow 4f)$ PL emission spectrum is a single broadband, centered at ~2.03 eV (610 nm) at room temperature.

PL spectroscopy is a useful characterization method for stimulable phosphors. PL has been observed from three of the four possible rare-earth ion charge states in SrS:Eu,Sm, namely Eu^{2+}, Sm^{3+}, and Sm^{2+}. The Eu^{2+} PL is excited by light in the ''write'' band as well as the ''read'' band.[2] The PL spectrum of the Sm^{3+} ions, which is centered at almost the same wavelength as the Eu^{2+} PL spectrum but consists of groups of narrow $(4f\rightarrow 4f)$ lines, has been observed with UV excitation.[4,5] PL from both the Eu^{2+} and Sm^{3+} ions is observed in the ground state of the charge-transfer system, in which all the Sm traps are depleted. On the other hand, the Sm^{2+} PL can occur only when some of the traps are filled, and thus indicates that the system is in a partially or fully ''written'' state. The Sm^{2+} PL should thus be especially useful as a probe of the dynamics of the optical storage process.

The PL from the Sm^{2+} ions in XS:Eu,Sm was first ob-

served in an article by Keller[6] (in 1959). In this previous work, a broad infrared PL emission band was observed, with a peak at ~0.73 eV (1700 nm), under conditions of simultaneous visible excitation (tungsten source) and UV excitation (xenon arc lamp source) at $T=77$ K. The infrared PL could not be observed at room temperature due to thermal quenching of the PL intensity. To our knowledge, no further studies of the infrared Sm^{2+} PL in *X*S:Eu,Sm stimulable phosphors were done after this initial report. In the present study, we expand on the work of Keller[6] by carrying out a more extensive investigation of the properties of the Sm^{2+} PL in bulk ceramic SrS:Eu,Sm. PL was excited by visible lasers at 2.33 eV (532 nm), 2.41 eV (514.5 nm), and 2.54 eV (488 nm); an infrared laser at 1.165 eV (1064 nm); and a wavelength-tunable, monochromatized xenon arc lamp source. The temperature dependence of the PL intensity, peak emission energy, and spectral linewidth and line shape was measured from 14 to 300 K. The xenon source was used to obtain the excitation spectrum of the Sm^{2+} PL, at $T=14$ K, from 1.7 to 6.2 eV (200 to 730 nm). The dependence of the PL emission intensity on excitation intensity was measured at each of the three visible laser wavelengths. Finally, the time dependence of the PL was examined under conditions of visible laser excitation followed by infrared laser excitation, and the Sm^{2+} PL intensity was found to decay slowly with time for these conditions.

The present study confirms the principal results of the earlier work,[6] the peak emission energy and linewidth of the PL emission spectrum at low temperature and the thermal quenching of the PL from 77 K to room temperature. However, we observed that the Sm^{2+} PL is excited by steady-state irradiation at a single wavelength, either visible or UV, and that simultaneous irradiation at two wavelengths is not needed. Also, the more extensive results of the present study, combined with an improved understanding of the energy levels and optical transitions of divalent rare-earth ions,[7,8] support a somewhat different model for the Sm^{2+} PL process than the model proposed by Keller.[6]

The results of the present study confirm that the infrared Sm^{2+} PL is a probe of the ''written'' state of the optical storage system in a stimulable phosphor that contains Sm as the trap species. It is hoped that this work will encourage further PL investigations of the dynamics of the optical storage process in Sm-containing stimulable phosphors, including technologically important thin-film structures as well as bulk ceramics.

II. EXPERIMENTAL PROCEDURE

For this study, SrS was doped with 200 parts per million by weight (ppmw) Eu and 200 ppmw Sm. Dopants were introduced as $EuCl_3$ and $SmCl_3$. A sintering flux of 4 wt. % LiF and 2 wt. % Li_2CO_3 was added to facilitate incorporation of the Eu and Sm dopants into the host. The material was mixed by ball milling and fired at 1173 K for 1 h in a nitrogen atmosphere to form a solid ceramic specimen. The specimen was mounted in a liquid-helium optical cryostat with fused-silica windows that provided temperature control from 4 to 300 K. The infrared PL was detected by a PbS photoconductive detector with integrated preamplifier and thermoelectric cooler. Several light sources were used to excite the PL: first, a CW Ar^+ laser operating at 2.41 eV (514.5 nm) or 2.54 eV (488 nm); second, a pulsed Nd:YAG laser operating at 1.165 eV (1064 nm), 2.33 eV (532 nm), or 4.66 eV (266 nm); and third, a lamp-monochromator source, consisting of a 400 W Xe arc lamp and a 0.22 m double monochromator, for low-intensity wavelength-tunable excitation within a 1.7–6.2 eV (200–720 nm) range. The wavelength resolution of the lamp-monochromator source, with 1200 line/mm gratings and 2 mm slit widths, was 4 nm; the photon energy resolution thus varied from 0.01 eV at 1.7 eV to 0.12 eV at 6.2 eV. The Ar^+ laser and lamp-monochromator source were chopped at 20 Hz with a mechanical chopper, and the Nd:YAG laser was pulsed at 20 Hz. Maximum intensity (or photon flux) incident on the specimen, averaged over the pulse or chopper repetition period, was 2.9 W/cm^2 (7.5×10^{18} photons/sec/cm^2) at 2.41 eV and 2.6 W/cm^2 (6.4×10^{18} photons/sec/cm^2) at 2.54 eV for the Ar^+ laser; 2.6 W/cm^2 at 1.165 eV (1.4×10^{19} photons/sec/cm^2), 0.47 W/cm^2 (1.3×10^{18} photons/sec/cm^2) at 2.33 eV, and 0.34 W/cm^2 (4.6×10^{17} photons/sec/cm^2) at 4.66 eV for the Nd:YAG laser. The maximum intensity of the lamp-monochromator source was 3.6×10^{-6} W/cm^2. (The incident intensity values have uncertainties of roughly 20% due to the uncertainty of the measured beam areas; the relative uncertainty of different intensities within a single set of measurements is much smaller.)

For measurements of the PL emission spectrum, the time dependence, and the low-temperature intensity dependence (variation of emission intensity with excitation intensity), two pairs of mirrors were used to collect and focus the PL onto the entrance slit of a 0.6 m spectrometer with a 300 line/mm grating blazed at 2000 nm and slit widths set to 3 mm. The PbS detector was attached to the spectrometer exit slit, and an infrared longpass filter was used to reject wavelengths below 1200 nm. The wavelength resolution of this spectrometer was 17 nm, corresponding to a photon energy resolution of 0.007 eV at the peak emission energy of 0.7 eV. For measurements of the PL excitation spectrum, the room-temperature intensity dependence, and the temperature dependence of the total PL intensity, this spectrometer was not used. Instead, the PbS detector was mounted near the cryostat, after the first pair of mirrors, and the infrared longpass filter was placed in front of the detector.

The wavelength variation of the response function of the spectrometer/PbS detector system, from 0.52 to 1.04 eV (1200 to 2400 nm), was determined by measuring the response of this system to a 200 W tungsten-halogen lamp that had been calibrated against a NIST irradiance standard lamp.[9] Knowledge of the system response function allowed us to normalize the PL emission spectra to dimensions of (number of emitted photons)/(unit photon energy interval). The output power of the lamp-monochromator source, from 1.7 to 6.2 eV, was determined by measuring the response of a NIST-calibrated Si photodiode[10] to this source. Knowledge of the source power (or photon flux) allowed us to normalize the PL excitation spectrum to dimensions of (number of emitted photons)/(number of exciting photons).

A lock-in amplifier provided phase-sensitive detection of the PbS detector signal at the 20 Hz source modulation frequency. Experiments were computer-controlled by a personal computer system, which scanned the wavelength of the

0.6 m spectrometer (for emission spectra) or the lamp-monochromator source (for the excitation spectrum) and recorded the output from the lock-in amplifier. For slow time-resolved measurements ($t>1$ s) of the PL intensity, which were needed to observe the PL time dependence for ''write'' (2.33, 2.41, or 2.54 eV) excitation followed by ''read'' (1.165 eV) excitation, the lock-in amplifier output voltage was recorded as a function of time on a digital oscilloscope.

III. RESULTS

Sm^{2+} PL emission spectra at twelve temperatures between 13 and 301 K, excited by the Ar^{+} laser at 2.54 eV, with 0.16 W (3.9×10^{17} photons/s) average power at the specimen and 20 Hz chopping frequency, are shown in Fig. 1(a). The same set of spectra is plotted again in Fig. 1(b), rescaled to equalize the peak intensity of each spectrum, in order to better display the temperature dependence of the linewidth and line shape. As a function of increasing temperature, the emission intensity decreases, and the peak emission energy and linewidth increase. In order to examine these trends more quantitatively, a nonlinear least-squares curve fitting procedure was used to fit each of the observed spectra with a skewed-Gaussian line-shape function that has been described previously.[11] To illustrate the quality of the fits, in Fig. 1(c) the fitted line-shape functions (thick dashed lines) are plotted together with the observed spectra (thin solid lines) at two temperatures.

The temperature dependence of the total, spectrally integrated, Sm^{2+} PL intensity, measured at 23 temperatures between 12 and 297 K, is plotted in Fig. 2(a). The excitation conditions were the same for the temperature dependence shown in Fig. 2(a) as for the emission spectra shown in Fig. 1, except that the average laser power was reduced to 1.5 mW (3.8×10^{15} photon/s). (Lower laser power was needed to obtain a good signal-to-noise ratio for measurements of the spectrally integrated PL intensity than for measurements of the emission spectrum.) The intensity (I_{PL}), plotted on a semilogarithmic scale in Fig. 2(a), is seen to decrease monotonically with increasing temperature. Two trial functions were fitted to the observed temperature dependence. The first function represents thermally activated quenching with a single activation energy,

$$I_{\mathrm{PL}}(T)=I_{\mathrm{PL}}(0)/[1+A\ \exp(-E_A/k_BT)]. \qquad (1)$$

The best fit of Eq. (1) to the data, with $A=420\pm270$ and $E_A=0.094\pm0.015$ eV, is shown as a dashed line in Fig. 2(a). The second function represents a sum of two thermally activated quenching processes,

$$I_{\mathrm{PL}}(T)=I_{\mathrm{PL}}(0)/[1+A1\ \exp(-E_{A1}/k_BT)+A2\ \exp(-E_{A2}/k_BT)]. \qquad (2)$$

The best fit of Eq. (2) to the data, with $A1=3.3\pm1.0$, $E_{A1}=0.016\pm0.004$ eV, $A2=2600\pm1000$, and $E_{A2}=0.132\pm0.010$ eV, is shown as a dash-dotted line in Fig. 2(a). It is apparent from inspection of Fig. 2(a) that Eq. (2) fits the data significantly better than Eq. (1); the weighted sum of squared errors (SSE), which is a quantitative measure of the deviation between the data and the fitted function, is 18 times larger for Eq. (1) than for Eq. (2). A third trial function, with three distinct activation energies, was found not to fit the data significantly better than Eq. (2). The function of Eq. (2), with two activation energies, thus appears to provide a good description of the temperature dependence of the intensity.

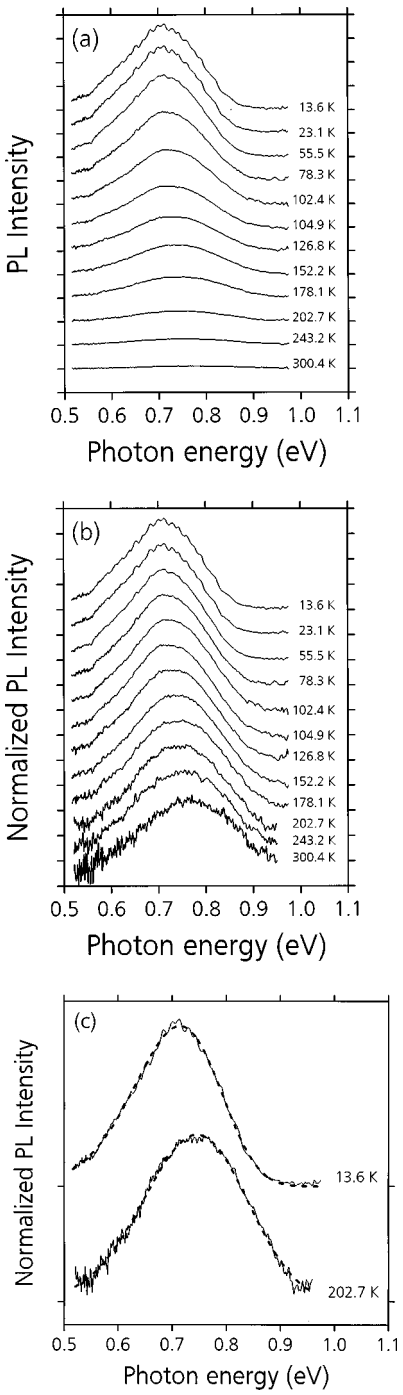

FIG. 1. (a) SrS:Sm^{2+} PL emission spectra at twelve temperatures between 13 and 300 K, excited by an Ar^{+} laser at 2.54 eV, 20 Hz chopping frequency, and 0.89 W/cm^2 time-averaged excitation intensity. Spectra are offset vertically to improve visibility. (b) PL emission spectra, same set of data as in Fig. 5(a), multiplied by scale factors chosen to equalize the peak intensities. (c) PL emission spectra at two temperatures, illustrating curve-fitting results. The experimental data are shown as solid lines and the fitted skewed-Gaussian line-shape functions are shown as dashed lines.

[The uncertainty in a parameter such as E_{A1} is defined as the deviation from the best-fit value that causes a statistically

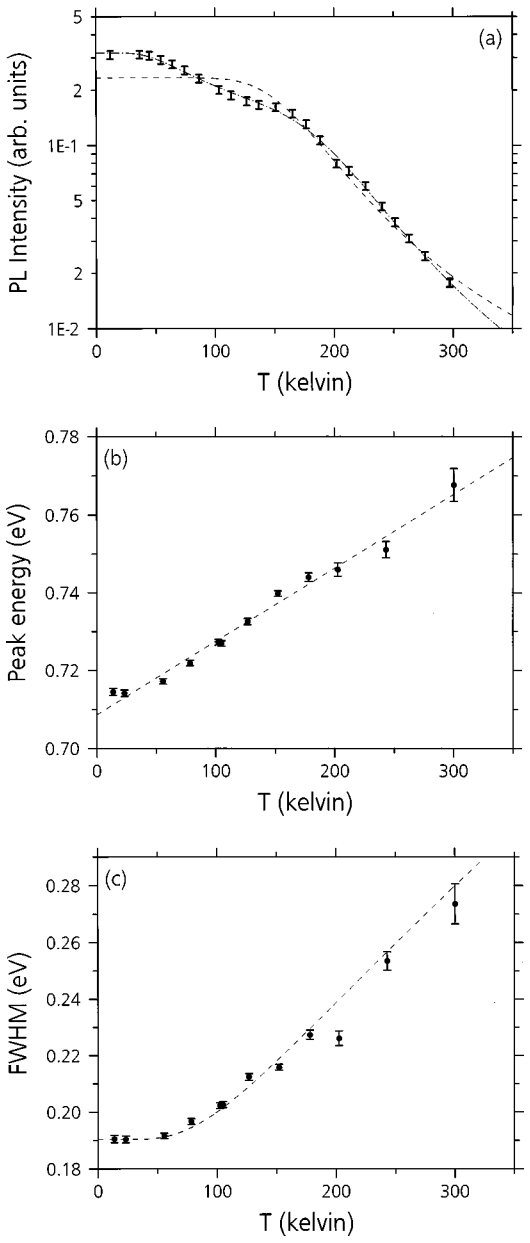

FIG. 2. (a) Total, spectrally integrated SrS:Sm^{2+} PL intensity as a function of temperature, plotted on a semilogarithmic scale. Data points are plotted as vertical error bars, the fitted function $I_{PL}(T) = I_0/[1+A\exp(-E_A/k_BT)]$ is plotted as a dashed curve, and the fitted function $I_{PL}(T) = I_0/[1+A1\exp(-E_{A1}/k_BT) + A2\exp(-E_{A2}/k_BT)]$ is plotted as a dash-dotted curve. (b) Peak energies of SrS:Sm^{2+} PL emission spectra vs temperature. Data points are plotted as circles with error bars; the linear fit $E_{PL}(T) = E_0 + E_1T$ is plotted as a dashed line. (c) Full widths at half maximum (FWHM) of SrS:Sm^{2+} PL emission spectra vs temperature. Data points are plotted as circles with error bars; the fitted function $W(T) = W_0[\tanh(\Omega/2k_BT)]^{-1/2}$ is plotted as a dashed curve.

significant increase in the SSE, specifically $\mathrm{SSE}(x_0 \pm \Delta x)/\mathrm{SSE}(x_0) = (N-P+4)/(N-P)$, where x_0 is the best-fit value of parameter x, Δx is the uncertainty in x, N is the number of fitted data points, and P is the number of adjustable parameters [e.g., $P=5$ in Eq. (2)]. With this definition, the calculated uncertainty Δx should represent a 2σ deviation; i.e., there is a 95% probability that the actual value of x lies within the range $(x_0 \pm \Delta x)$. This definition of the uncertainty in the value of a fitted parameter is used throughout the present study.]

The peak energies and full widths at half maximum (FWHM) of the PL emission spectra, taken from the fitted line-shape functions [as shown in Fig. 1(c)], are plotted as functions of temperature in Figs. 2(b) and 2(c), respectively. In Fig. 2(b), the peak energy is seen to increase as a linear function of temperature,

$$E_{PL}(T) = E_{PL}(0) + E_1T, \tag{3}$$

with $E_{PL}(0) = 0.709 \pm 0.002$ eV and $E_1 = (1.9 \pm 0.2) \times 10^{-4}$ eV/K. The fit is shown as a dashed line.

Figure 2(c) shows the temperature dependence of the FWHM of the PL emission spectrum. The FWHM is seen to increase with temperature above 50 K. The temperature dependence of the FWHM, $W(T)$, was fitted by a function derived from an electron-phonon coupling model[12] discussed in the next section,

$$W(T) = W(0)[\tanh(\Omega/(2k_BT))]^{-1/2}, \tag{4}$$

with $W(0) = 0.190 \pm 0.004$ eV and $\Omega = 0.026 \pm 0.001$ eV. The fitted function is shown as a dashed line.

An oscillatory fine structure, not accounted for by the fitted skewed-Gaussian line shapes, occurs in the lower-temperature spectra in Fig. 1. To better display this fine structure, the fitted line-shape functions were subtracted from the experimental data. The results of this subtraction are shown in Fig. 3(a) for the five spectra recorded at temperatures between 13 and 103 K. The amplitude of the oscillatory structure decreases rapidly with increasing temperature.

The frequency content of the oscillations shown in Fig. 3(a) was determined by Fourier analysis. The Fourier transforms of the spectra from Fig. 3(a) are plotted in Fig. 3(b). The oscillation period, or inverse of the Fourier frequency, has units of eV, and the Fourier frequency thus has units of $(\mathrm{eV})^{-1}$. Significant frequencies in Fig. 3(b) are indicated by arrows labeled ''*A*'' to ''*E*.'' Arrows *A*, *B*, and *C* point to the observed peaks in the transform spectra, with frequencies of roughly $(0.0155\ \mathrm{eV})^{-1}$, $(0.028\ \mathrm{eV})^{-1}$, and $(0.100\ \mathrm{eV})^{-1}$. Peaks *A* at $(0.0155\ \mathrm{eV})^{-1}$ and *B* at $(0.028\ \mathrm{eV})^{-1}$ are prominent at the lowest temperatures, but become unobservable at temperatures higher than 60 K. Peak *C* at $(0.100\ \mathrm{eV})^{-1}$ persists to higher temperature than peaks *A* and *B*. Arrow *D* indicates a Fourier frequency of $(0.026\ \mathrm{eV})^{-1}$, which corresponds to the parameter $\Omega = 0.026$ eV from Eq. (4). Arrow *E* indicates a Fourier frequency of $(0.0352\ \mathrm{eV})^{-1}$, which corresponds to the longitudinal optical (LO) phonon, the highest-energy vibrational mode of the SrS lattice.[13] The interpretation of the Fourier transform spectra will be discussed further below.

The excitation spectrum of the Sm^{2+} PL at $T = 14$ K, from 1.7 to 6.2 eV, is shown in Fig. 4. This spectrum was excited by the lamp-monochromator source, as discussed above. The function used to fit the excitation spectrum, shown as a solid curve, is a sum of four Gaussian peaks and a quadratic background component. The relative excitation efficiencies (peak heights), the peak energies, and the FWHM's of the fitted peaks are listed in Table I.

The dependence of the PL intensity (I_{PL}) on visible-laser excitation intensity (I_{ex}) was examined at low temperature and room temperature. The low-temperature ($T = 20$ K)

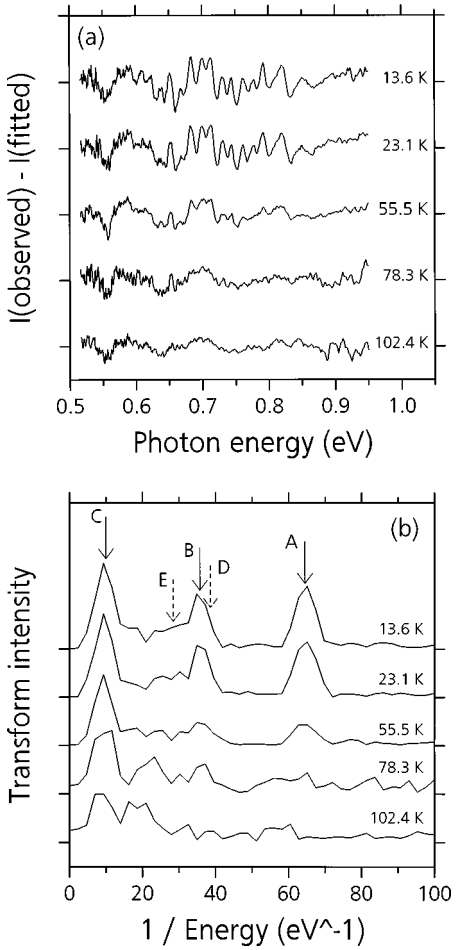

FIG. 3. (a) Difference spectra obtained by subtracting the fitted skewed-Gaussian line shape functions from the measured SrS:Sm^{2+} PL spectra at temperatures between 13 and 103 K. Note the oscillatory structure in the lower-temperature spectra. (b) Fourier transforms of the difference spectra shown in (a). Arrows *A*, *B*, and *C* show oscillations with Fourier frequencies of $(0.0155\,\mathrm{eV})^{-1}$, $(0.028\,\mathrm{eV})^{-1}$, and $(0.100\,\mathrm{eV})^{-1}$, respectively. The Fourier frequency is the inverse of the oscillation period. Arrow *D* shows the Fourier frequency of the parameter $\Omega = 0.0259$ eV obtained from the fit to the FWHM data [Fig. 2(c)]. Arrow *E* shows the Fourier frequency of the 0.0352 eV SrS longitudinal optical (LO) phonon mode.

intensity-dependent data, measured at an emission energy of 0.73 eV, near the peak of the emission spectrum, are shown in Fig. 5(a). For excitation with the pulsed Nd:YAG laser at 2.33 eV, the PL appears to saturate at high excitation intensity. (It should be emphasized that all the excitation intensities shown in Fig. 5 are time-averaged intensities, with respect to the pulsed laser or mechanical chopper duty cycle, rather than peak intensities.) The intensity dependence for Nd:YAG excitation was fitted by the function [shown as a solid curve in Fig. 5(a)],

$$I_{\mathrm{PL}}(I_{\mathrm{ex}}) = I_{\mathrm{PL}}(\infty) I_{\mathrm{ex}} / (I_{\mathrm{sat}} + I_{\mathrm{ex}}), \tag{5}$$

where $I_{\mathrm{PL}}(\infty)$ is the saturation value of the PL intensity, and I_{sat} is the excitation intensity at the knee of the saturation curve. The fitted value of I_{sat} is $(5.8 \pm 0.8 \pm 1.2) \times 10^{16}$ photons/s/cm^2. The first quoted uncertainty is the statistical uncertainty of the fit, the second quoted uncertainty arises from the measurement of the excitation beam area.

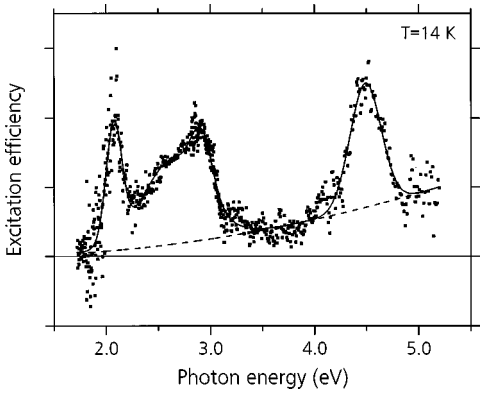

FIG. 4. SrS:Sm^{2+} PL excitation spectrum, measured at $T = 14$ K, excited by a lamp-monochromator source. The displayed spectrum is normalized to dimensions of (number of emitted photons)/(number of incident photons). Data are plotted as squares; the fitted function, a sum of four Gaussian peaks and a quadratic background, is plotted as a solid line; and the background is plotted as a dashed line. The efficiencies, peak energies, and FWHMs of the fitted Gaussian peaks are listed in Table I.

For excitation with the CW Ar^+ laser, the well-defined saturation behavior described by Eq. (5) was not observed, but the power dependence was found to be sublinear, suggesting that saturation effects are present in this case also. The Ar^+ data were fitted by power-law functions [dashed curves in Fig. 5(a)]

$$I_{\mathrm{PL}}(I_{\mathrm{ex}}) = \kappa (I_{\mathrm{ex}})^{\beta} \tag{6}$$

with power-law exponent $\beta = 0.77$ for excitation at 2.41 eV and $\beta = 0.85$ for excitation at 2.54 eV.

The room-temperature intensity dependence data are shown in Fig. 5(b). To compensate for the weak PL signal in these measurements, the PL was spectrally integrated in the same manner as for the excitation spectrum (Fig. 4). Less saturation is apparent at room temperature than at low temperature, i.e., the intensity dependencies are closer to linear within the examined range. The intensity dependence for 2.33 eV Nd:YAG excitation was fitted by Eq. (5) with $I_{\mathrm{sat}} = (1.10 \pm 0.23 \pm 0.22) \times 10^{18}$ photon/s/cm^2 (solid curve). (Note, however, that all the data points lie in the range $I_{\mathrm{ex}} < I_{\mathrm{sat}}$, which casts some doubt on the reliability of the fit. To accurately determine I_{sat}, the measurement range should encompass intensities both less than and greater than I_{sat}.) The intensity dependence for Ar^+ laser excitation, at both 2.41 and 2.54 eV, was fitted by a single power-law function with power-law exponent $\beta = 0.92$ (dashed curve).

Sm^{2+} PL was also excited by the Nd:YAG fundamental at 1.165 eV. With 1.165 eV excitation, however, the PL intensity was found to decay on a time scale of seconds to minutes. The infrared PL became too weak to observe after prolonged 1.165 eV excitation, but was restored after a brief period of visible (2.33, 2.41, or 2.54 eV) laser excitation. To quantify this behavior, the specimen was first irradiated for several minutes by the 2.33 eV laser beam, to saturate the Sm^{2+} population, then the 2.33 eV beam was blocked and the specimen was irradiated by the 1.165 eV beam. The av-

TABLE I. Fitted efficiencies, peak energies, and full widths at half maximum (FWHM) of the component peaks of the Sm^{2+} PL excitation spectrum, measured at $T=14$ K. Peak energies and FWHM's are given in both photon energy (eV) and wavelength (nm) units.

Peak no.	Efficiency (relative)	Peak photon energy (eV)	FWHM (eV)	Peak wavelength (nm)	FWHM (nm)
1	0.939	2.076 ± 0.006	0.180 ± 0.016	597	52
2	0.687	2.651 ± 0.050	0.698 ± 0.097	468	123
3	0.439	2.919 ± 0.018	0.229 ± 0.062	425	33
4	1	4.492 ± 0.016	0.353 ± 0.041	276	22

erage excitation intensity was 0.35 W/cm^2 (9.4×10^{17} photon/s/cm^2) at 2.33 eV and 1.6 W/cm^2 (8.9×10^{18} photon/s/cm^2) at 1.165 eV, and the specimen temperature was 14 K. The time dependence of the PL intensity at an emission energy of 0.73 eV, near the peak of the emission spectrum, was measured by a lock-in amplifier and recorded on the digital oscilloscope. The time decay of the PL is shown in Fig. 6 for times $t>1$ s, where $t=0$ corresponds to the onset of the 1.165 eV laser irradiation. (The measured time dependence at times $t<1$ s, not shown, was dominated by the instrumental response of the lock-in amplifier.) Decay curves similar to the one shown in Fig. 6 were obtained for initial irradiation at 2.41 or 2.54 eV, followed by irradiation at 1.165 eV.

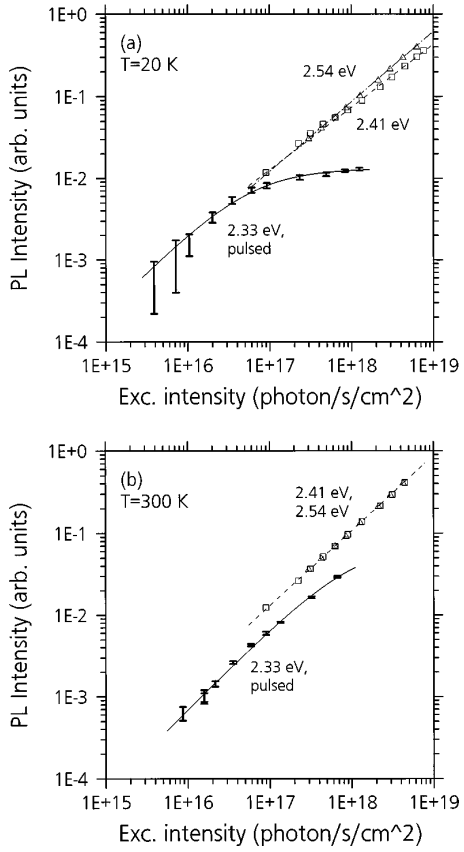

FIG. 5. (a) Excitation intensity dependence of the SrS:Sm^{2+} PL intensity at $T=20$ K, plotted on a double-logarithmic scale. The PL was measured at 0.73 eV, near the peak of the emission spectrum. Data points are plotted as vertical error bars for 2.33 eV pulsed Nd:YAG laser excitation, as squares for 2.41 eV CW Ar^+ laser excitation, and as triangles for 2.54 eV CW Ar^+ laser excitation. The function $I_{PL}(I_{ex})=I_{PL}(\infty)I_{ex}/(I_{sat}+I_{ex})$, fitted to the 2.33 eV Nd:YAG data, is shown as a solid line. Power-law fits to the 2.41 and 2.54 eV Ar^+ data are shown as dashed and dash-dotted lines. (b) Excitation intensity dependence of the SrS:Sm^{2+} PL intensity at $T=300$ K, plotted on a double-logarithmic scale. Data and fitted functions are plotted in the same manner as in (a). The dashed line represents a unified power-law fit to both the 2.41 eV data and the 2.54 eV data.

IV. DISCUSSION

The large FWHM of the Sm^{2+} ($5d\rightarrow4f$) PL spectrum (Fig. 1) and the temperature dependence of the FWHM [Fig. 2(c)] are indicative of strong electron-phonon coupling.[12] Indeed, the $(4f^{n-1})(5d)$ to $(4f^n)$ optical transitions of divalent rare-earth ions in crystals,[7,8] including the Eu^{2+} ion[5] in XS:Eu,Sm, generally show strong electron-phonon coupling. We will use a simple, semiclassical model, where the electron-phonon coupling is pictured as a change in the local atomic configuration (interatomic distances and bond angles) around the PL center, to analyze the line shape and temperature dependence of the PL spectrum. The key assumptions are that the electron-phonon coupling is one-dimensional (the dependencies of the electronic energy levels on the local atomic configuration are represented by functions of a single

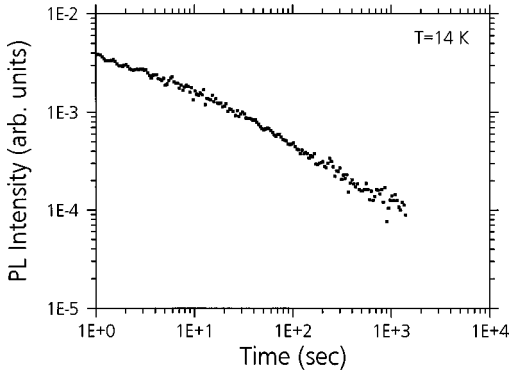

FIG. 6. Time dependence of the SrS:Sm^{2+} PL intensity for 1.165 eV laser excitation after an initial period of 2.33 eV laser excitation. The time-averaged incident intensity was 0.35 W/cm^2 at 2.33 eV and 1.6 W/cm^2 at 1.165 eV, the temperature was 14 K, and the PL was measured at 0.73 eV, near the peak of the PL emission spectrum. The time-dependence curve is plotted on a double-logarithmic scale, where $t=0$ corresponds to the onset of 1.165 eV laser excitation.

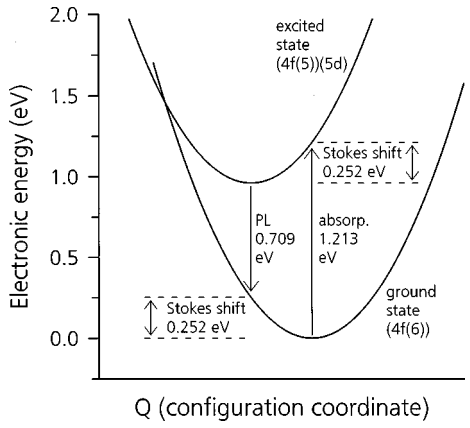

FIG. 7. Energy-level diagram for linear electron-phonon coupling model of the lowest ($5d \rightleftarrows 4f$) optical transitions of the SrS:Sm^{2+} center.

''configuration coordinate,'' denoted Q) and linear (the ground-state and excited-state energies are quadratic functions of Q with the same curvature, hence the difference between the ground- and excited-state energies is a linear function of Q). An energy-level diagram for this model is shown in Fig. 7.

The energy of the coupled phonon (Ω) can be determined from the temperature dependence of the FWHM of the PL spectrum $[W(T)]$, according to Eq. (4). The value $\Omega = 0.026 \pm 0.001$ eV was obtained by fitting Eq. (4) to the $W(T)$ data. Another way to determine the coupled phonon energy (or energies) is from the spacing of the phonon replica peaks that may appear in the PL spectrum, especially at low temperature.[12] We attribute the oscillations in the low-temperature spectrum of the SrS:Sm^{2+} center, which are prominent in the subtracted spectra shown in Fig. 3(a), to such phonon replicas. The Fourier analysis of the low-temperature spectra, Fig. 3(b), shows that the phonon replicas arise from two distinct coupled modes, with energies (equal to the spacings between the peaks) $\Omega_1 = 0.0155$ eV and $\Omega_2 = 0.028$ eV. The energy of the Ω_2 mode lies between the transverse optical (TO) and longitudinal optical (LO) phonon energies in SrS, which were determined to be 0.02405 and 0.0352 eV, respectively, by far-infrared absorption spectroscopy;[13] the Ω_2 mode thus probably has an optical-phonon-like character. The similarity of the energies of the $\Omega_2 = 0.028$ eV (determined from the phonon replica spacing) and $\Omega = 0.026$ eV (determined from the temperature dependence of the FWHM) phonon modes suggests that these are really the same mode, observed by two methods; the spectroscopic determination of the energy, from the replica spacing, is expected to be the more accurate determination.

The observation of two coupled modes indicates that the electron-phonon coupling is more complex than assumed by the one-dimensional model. For simplicity, however, we will continue to analyze the results in terms of the one-dimensional model. We will assume that the higher-energy (Ω_2) phonon, which apparently controls the thermal broadening of the PL, also determines the magnitude of the other electron-phonon coupling effects, to be discussed.

A key parameter of the electron-phonon coupling model is the Stokes shift (E_S), which is the difference between the zero-phonon energy, $U(T)$ (defined as the electronic energy difference between the ground and excited states of the PL center, in the absence of electron-phonon coupling) and the peak of the PL emission spectrum, $E_{\mathrm{PL}}(T)$,

$$E_{\mathrm{PL}}(T) = U(T) - E_S . \tag{7}$$

(We write $E_{\mathrm{PL}}(T)$ and $U(T)$ to emphasize that the peak energy is a function of temperature, as shown in Fig. 2(b).) According to the model, if the coupled phonon energy (Ω) and the low-temperature value of the FWHM $[W(0)]$ are known, then the Stokes shift is given by

$$E_S = [W(0)]^2/[8 \ln(2) \Omega]. \tag{8}$$

Substituting the values $W(0) = 0.190 \pm 0.004$ eV and $\Omega = 0.028 \pm 0.001$ eV into Eq. (8) yields $E_S = 0.233 \pm 0.011$ eV; substituting $E_{\mathrm{PL}}(0) = 0.709 \pm 0.002$ eV and E_S into Eq. (7) yields $U(0) = 0.942 \pm 0.011$ eV. Another important model parameter is the electron-phonon coupling strength (S), a dimensionless number that represents the average number of phonons created during lattice relaxation subsequent to the electronic transition. The coupling strength is given in terms of the other parameters by

$$S = E_S/\Omega = [W(0)]^2/[8 \ln(2) \Omega^2]. \tag{9}$$

From the above results, the value of S is found to be 8.3 ± 0.5. When S is small, the PL spectrum is expected to show an observable zero-phonon line (a narrow peak at the zero-phonon energy). When S is large, typically greater than 5, as in the present case, the zero-phonon line is expected to be too weak to observe.

Another prediction of the model is that the peak energy for optical absorption from the ground to the excited state of the PL center, $E_{\mathrm{abs}}(T)$, is shifted up from the zero-phonon energy by the Stokes shift E_S (see Fig. 7),

$$E_{\mathrm{abs}}(T) = U(T) + E_S = E_{\mathrm{PL}}(T) + 2E_S . \tag{10}$$

The absorption peak is thus predicted to occur at 1.175 ± 0.022 eV at $T = 0$ K, or 1.232 ± 0.023 eV (1006 ± 19 nm) at $T = 300$ K (room temperature). One experimental probe of the ground-to excited-state absorption of the Sm^{2+} ions is the IR-stimulated ''read'' process, Sm→Eu electron transfer followed by photon emission from the regenerated Eu^{2+} ions. The peak of the room-temperature ''read'' excitation spectrum has been experimentally determined[14] to occur at 1.253 ± 0.014 eV (989 ± 11 nm), in good agreement with the SrS:Sm^{2+} optical absorption peak predicted by the linear electron-phonon coupling model. In addition to supporting the validity of the model, the accuracy of this prediction also shows that the initial state for the ''read'' process is the same as the excited state of the SrS:Sm^{2+} PL center.

The linear increase of $E_{\mathrm{PL}}(T)$ shown in Fig. 2(b), and represented by the coefficient $E_1 = 1.9 \times 10^{-4}$ eV/K in Eq. (3), is not predicted by the electron-phonon coupling model. This increase is attributed to a reduction in the crystal field around the Sm^{2+} ion with increasing temperature due to thermal expansion of the lattice.[7] The reduction in the crystal field causes an increase in the energy of the lowest $(4f^5) \times (5d)$ excited state, and thus in the zero-phonon energy $U(T)$ and in $E_{\mathrm{PL}}(T)$ and $E_{\mathrm{abs}}(T)$. (See, for example, the

energy level diagram in Fig. 2 of Ref. 8.) This model predicts the correct sign for the temperature coefficient E_1.

The thermally activated quenching of the PL, shown in Fig. 2(a), is also ascribed to the electron-phonon coupling. Qualitatively, there is assumed to be an energy barrier to nonradiative recombination, which can be overcome, at sufficiently high temperature, by the absorption of thermally generated phonons. As pointed out above, the experimental $I_{\rm PL}(T)$ data are fit much better by a function with two different activation energies for thermal quenching [Eq. (2)], $E_{A1}=0.016\pm0.004$ eV and $E_{A2}=0.132\pm0.010$ eV, than by a function with a single activation energy [Eq. (1)]. We speculate that there is a correlation between the occurrence of two coupled phonon modes, $\Omega_1=0.0155$ eV and $\Omega_2=0.028$ eV, as seen in the Fourier transform analysis of the phonon replicas [Fig. 3(b)], and the observation of two activation energies in the thermal quenching data, because each coupled phonon mode may give rise to a distinct thermally activated nonradiative recombination process.

A formal prediction of the activation energy for nonradiative recombination is obtained from the linear electron-phonon coupling model (assuming, once again, that the Ω_2 phonon mode is the strongly coupled mode) by attributing the nonradiative recombination process to the crossing of the ground-state and excited-state configuration coordinate curves (see Fig. 7). The activation energy ($E_{A,\rm model}$) is then predicted to be the energy difference between the minimum of the excited-state curve, and the energy where the two curves cross, which is

$$E_{A,\rm model}=[U(0)-E_S]^2/(4E_S)=0.54\ \text{eV}. \qquad (11)$$

The activation energy predicted by Eq. (11) is about four times larger than the observed activation energy of the dominant nonradiative process, $E_{A2}=0.132\pm0.010$ eV. However, it is well known that the simple, linear electron-phonon coupling model does not (in most cases) accurately predict the activation energy for nonradiative recombination, because this model neglects anharmonic terms in the potentials $U(Q)$, which may greatly increase the overlap between the higher vibrational levels of the ground and excited electronic states, and thus reduce the nonradiative activation energy.[8] (If the anharmonic terms were known, then a more accurate prediction of the activation energy could be obtained from a full quantum-mechanical calculation.)

It is interesting to compare the electron-phonon coupling at the SrS:Sm^{2+} center with the electron-phonon coupling at the Eu^{2+} center in MgS, CaS, or CaSe, which has been previously studied.[15] The PL is believed to arise from $4f\rightarrow5d$ transitions both for the X(S,Se):Eu^{2+} centers and for SrS:Sm^{2+}. *A priori*, one might expect the magnitude of the electron-phonon coupling to be similar for the Eu^{2+} and Sm^{2+} centers because of the similarity of the electronic transitions and the host crystals. However, the electron-phonon coupling was actually found to be significantly smaller for X(S,Se):Eu^{2+} than we find for SrS:Sm^{2+}. From Figs. 2 and 4 of Ref. 15, the coupled phonon energy (Ω), coupling strength (S), and Stokes shift (E_S) are estimated to be $\Omega=0.0409$ eV, $S=2$, and $E_S=0.082$ eV for MgS:Eu^{2+}; $\Omega=0.0335$ eV, $S=3$, and $E_S=0.100$ eV for CaS:Eu^{2+}; and $\Omega=0.0174$ eV, $S=5$, and $E_S=0.087$ eV for CaSe:Eu^{2+}; whereas for SrS:Sm^{2+} we find $\Omega=0.028$ eV, $S=8.3$, and $E_S=0.232$ eV. (The zero-phonon line is observed in the PL spectra of the Eu^{2+} centers; we thus define E_S for these centers as the energy difference between the narrow zero-phonon line and the peak of the broad multiphonon band.)

We suggest two possible mechanisms for the increased Stokes shift in SrS:Sm^{2+} as compared to X(S,Se):Eu^{2+}. First, the energies of the $5d$ orbitals of the Sm^{2+} ion may be degenerate with the SrS conduction band. This degeneracy will cause delocalization of the outer electron in the excited state of the PL center, which nominally has the electronic configuration $Sm^{2+}(4f^5)(5d)$. Therefore, the change in the electronic charge distribution from the ground to the excited state will be larger than in the absence of the degeneracy with the conduction band. The larger change in the charge distribution from the ground to excited state may, in turn, cause an increase in the electron-phonon coupling. Second, the incorporation of Sm^{3+} ions in a II-VI host crystal requires a charge compensation mechanism. (As discussed above, the stable Sm charge state is believed to be Sm^{3+} rather than Sm^{2+}.) The compensating defects or impurities may form complexes with the Sm ions, and the electron-phonon coupling may be stronger for the electronic transitions of the complex than for the corresponding transitions of an isolated Sm^{2+} ion.

There is a correlation between the thermal quenching of the steady-state PL intensity and the saturation behavior seen in the excitation intensity dependence curves, as shown in Figs. 5(a) and 5(b) and modeled by Eq. (5). Below saturation, the steady-state PL intensity [$I_{\rm PL}(T)$] is expected to vary with temperature in proportion to the ratio $\nu_r/[\nu_r+\nu_{\rm nr}(T)]$, where ν_r is the radiative recombination rate (which is temperature-independent in most systems), and $\nu_{\rm nr}(T)$ is the thermally activated nonradiative rate. On the other hand, the saturation value ($I_{\rm sat}$) of the excitation intensity ($I_{\rm ex}$) is expected to vary in direct proportion to the total recombination rate $\nu_r+\nu_{\rm nr}(T)$, as indicated by the rate equation model for saturation of a two-level system,

$$\partial n_{\rm ex}/\partial t=-\partial n_{\rm gr}/\partial t=\sigma I_{\rm ex}n_{\rm gr}-[\nu_r+\nu_{\rm nr}(T)]n_{\rm ex}, \qquad (12)$$

where $I_{\rm ex}$ is the excitation intensity (photons/cm^2/s), σ is the absorption cross section of the two-level system, $n_{\rm gr}$ is the ground-state population, and $n_{\rm ex}$ is the excited-state population. Thus, as a function of temperature, $I_{\rm sat}(T)$ should vary in inverse proportion to $I_{\rm PL}(T)$ (excited below saturation). From the curve fitted to the $I_{\rm PL}(T)$ data [Eq. (2)], the ratio of the PL intensity at $T=300$ K to the PL intensity at $T=20$ K is $I_{\rm PL}(300\ {\rm K})/I_{\rm PL}(20\ {\rm K})=(18.5)^{-1}$. From the discussion following Eq. (5), the corresponding ratio of the saturation intensities is $I_{\rm sat}(300\ {\rm K})/I_{\rm sat}(20\ {\rm K})=19\pm5$; these two ratios are inversely proportional, just as the rate model predicts.

The PL excitation spectrum, Fig. 4, provides information about the Sm^{2+} excited states and other electronic excited states of the SrS:Eu,Sm system. The peak at 2.08 eV is ascribed to a higher Sm^{2+} excited state. A peak at 2.1 eV (590 nm) was observed in the ''read'' excitation spectrum,[16] for electron transfer from Sm to Ce ions, in the SrS:Ce,Sm optical storage system. A peak at similar energy, 1.93 eV, was observed in the optical absorption spectrum[17] of SrS:Sm^{2+}.

The broad peak at 2.65 eV (or 468 nm), with FWHM of 0.7 eV (or 120 nm), is ascribed to optical absorption by the Eu^{2+} ions, followed by Eu→Sm electron transfer, i.e., the ''write'' process. The energy and width of this peak are similar to the parameters previously reported for the dominant peak in the ''write'' excitation spectrum.[2,14,18] The origin of the 2.92 eV peak is not known; this peak may arise either from a Sm^{2+} excited state or from a Eu^{2+} excited state. The UV peak at 4.49 eV is ascribed to SrS interband excitations, which may be either excitons or electron-hole pairs. The energy of this peak is similar to the energy of the lowest interband absorption peak in the powder absorption spectrum of undoped SrS, which was found[4] to be ~4.6 eV. To summarize, the PL excitation spectrum shows peaks due to optical absorption by the Sm^{2+} ions (correlated with the ''read'' process), absorption by the Eu^{2+} ions followed by Eu→Sm electron transfer (the ''write'' process), and above-band-gap excitation of the SrS host crystal.

As shown in Fig. 6, the Sm^{2+} PL can also be excited at 1.165 eV, which is close to the infrared ''read'' excitation peak at 1.25 eV. For intense laser excitation at 1.165 eV subsequent to visible laser excitation, the Sm^{2+} PL was observed to decay with time on a scale of seconds to minutes. The form of the time decay is approximately $I(t) \propto t^{-0.5}$ under the particular excitation conditions used for this experiment. This behavior can be qualitatively explained by stimulation of the ''read'' (Sm→Eu electron transfer) process by the IR laser excitation, which gradually depletes the Sm^{2+} population and thus reduces the Sm^{2+} PL intensity.

Finally, we provide a brief critique of the model first proposed[6] for the infrared PL in SrS:Eu,Sm and SrS:Ce,Sm. This earlier model is based on the assumption that the lowest-energy electronic state of Sm^{2+} has a $(4f^5)(5d)$ configuration, rather than $(4f^6)$ as we have assumed; further, electron-phonon coupling is not considered. According to the earlier model, the 2.1 eV absorption peak is due to a $(4f \rightarrow \text{conduction band})$ transition of the $Sm^{2+}(4f^5)(5d)$ configuration, which results in a $Sm^{3+}(4f^4)(5d)$ final state. The 1.25 eV ''read'' excitation peak (reported as 1.30 eV in Ref. 6) is due to a $(5d \rightarrow \text{conduction band})$ transition, which results in a $Sm^{3+}(4f^5)$ final state (effectively the Sm^{3+} ground state). Finally, the PL peak at 0.72 eV at $T=77$ K (reported as 0.75 eV in Ref. 6) is due to a $Sm^{3+}(4f^4)(5d) \rightarrow (4f^5)$ transition. The excited state of the PL center is identified with the final state of the 2.1 eV absorption process. According to this model, the infrared PL arises from an excited Sm^{3+} state that is created by the ionization of Sm^{2+}, whereas in our model the PL arises directly from a Sm^{2+} transition.

In view of our results, and other studies of rare-earth ions done subsequent to Ref. 6, the earlier model is seen to have significant flaws: (i) The Sm^{2+} ion has been studied in a number of host crystals, and the ground electronic configuration[7] is always $(4f^6)$, not $(4f^5)(5d)$. (ii) If the electron-trapping state were really $Sm^{2+}(4f^5)(5d)$, which has a weakly bound outer electron, rather than $Sm^{2+}(4f^6)$, then the long trapping lifetimes (many months in the dark at room temperature) would be difficult to explain. (iii) The model attributes the infrared PL to a $(5d) \rightarrow (4f)$ transition of Sm^{3+}, not Sm^{2+}, but the $(5d) \rightarrow (4f)$ transitions of trivalent rare-earth ions[7] generally occur in the vacuum UV. (iv) Our observation that the infrared PL is excited by 1.165 eV light contradicts the model, which holds that a photon energy of 1.165 eV is too low to excite the IR luminescence.

Most of the experimental results reported in Ref. 6 are consistent with the results of the present study and other recent work on optical storage systems. In Ref. 6, the Sm^{2+} PL was excited by simultaneous irradiation with 2.1 eV light and 4.4 eV (above-band-gap) light. This is consistent with our excitation spectrum (Fig. 4), which shows efficient excitation at both energies. Further (according to Ref. 6), when the 4.4 eV light is switched off and the 2.1 eV light is maintained, the infrared PL intensity ''slowly decays to zero'' in a time of ''the order of minutes.'' This indicates that the ''read'' process (net conversion of Sm^{2+} to Sm^{3+}) was induced by the 2.1 eV light, just as was observed in the present study (Fig. 6) for irradiation by 1.165 eV light. Other work[16] has shown that 2.1 eV light can induce the ''read'' process. The only experimental difference between the results of the present study and the results reported by Keller is that according to Keller ''when the [4.4 eV] light is maintained but the [2.1 eV] light is removed, there is no infrared emission,'' but our excitation spectrum shows efficient excitation of the Sm^{2+} PL at 4.4 eV without simultaneous irradiation at a second wavelength. Further work is needed to explain this discrepancy.

V. CONCLUSION

To summarize, infrared photoluminescence from the Sm^{2+} ions in a bulk ceramic specimen of the stimulable phosphor SrS:Eu,Sm was excited by visible (2.33, 2.41, and 2.54 eV) and infrared (1.165 eV) lasers and by a wavelength-tunable, monochromatized xenon arc lamp source. The temperature dependence of the infrared PL was examined from 14 to 300 K. The PL intensity was found to decrease monotonically with increasing temperature. The full width at half maximum of the PL emission spectrum, $W(T)$, was found to increase with temperature in a manner consistent with a linear electron-phonon coupling model, $W(T) = W_0[\tanh(\Omega/(2k_BT))]^{-1/2}$, with $W_0 = 0.190$ eV and coupled phonon energy $\Omega = 0.026$ eV. Periodic oscillations in the PL spectrum at $T < 60$ K provide direct evidence for coupling to two phonon modes, with phonon energies $\Omega_1 = 0.0155$ eV and $\Omega_2 = 0.028$ eV. The peak of the emission spectrum occurs at 0.709 eV (1750 nm) at 14 K and increases with temperature at a rate 1.9×10^{-4} eV/K. The PL peak shift is attributed to a decrease in the crystal field with increasing temperature. The electron-phonon coupling model predicts that the corresponding optical absorption peak, which is anti-Stokes shifted relative to the PL peak, should occur at 1.17 eV (1060 nm) at low temperature, or 1.23 eV (1010 nm) at room temperature. Previous measurements of the charge-transfer excitation spectrum in SrS:Eu,Sm showed a peak at 1.25 eV (990 nm), in good agreement with the model prediction. The PL excitation spectrum from 1.7 to 6.2 eV (200 to 730 nm) was measured at $T = 14$ K. Excitation peaks were observed at 2.076 eV (597 nm), ascribed to absorption to a higher excited Sm^{2+} state; at 2.651 eV (468 nm), ascribed to Eu^{2+} absorption followed by Eu→Sm charge transfer; at 2.919 eV (425 nm); and at 4.492 eV (276 nm), ascribed to interband excitation of the SrS. The infrared PL intensity was observed to decay with time, on a scale of

seconds to minutes, under 1.165 eV laser excitation subsequent to visible laser excitation at $T=14$ K. This decay is attributed to the Sm→Eu charge-transfer process.

The results reported here confirm that the infrared Sm^{2+} PL is a probe of the ''written'' state of the optical storage system in a stimulable phosphor that contains Sm as the trap species. It is hoped that this work will encourage further PL investigations of the dynamics of the optical storage process in Sm-containing stimulable phosphor materials that are currently being developed for optical data storage applications, including technologically important thin-film structures as well as bulk ceramics.

ACKNOWLEDGMENTS

The authors wish to thank George Storti, Tony Lewandowski, and Xuren Huang, Optex Communications, for their critical reading of the manuscript and insightful discussions, and Scott Matthews, Optex Communications, for his assistance in planning the project.

[1] J. Lindmayer, Solid State Technol. **31**, 125 (1988); Laser Focus World **25**, 119 (1989).
[2] S. P. Keller, J. E. Mapes, and G. Cheroff, Phys. Rev. **108**, 663 (1957).
[3] K. Chakrabarti, V. K. Mathur, J. F. Rhodes, and R. J. Abbundi, J. Appl. Phys. **64**, 1363 (1988).
[4] N. Yamashita and S. Asano, J. Phys. Soc. Jpn. **56**, 352 (1987).
[5] Y. Tamura and A. Shibukawa, Jpn. J. Appl. Phys., Part 1 **32**, 3187 (1993).
[6] S. P. Keller, Phys. Rev. **113**, 1415 (1959).
[7] G. H. Dieke, *Spectra and Energy Levels of Rare Earth Ions in Crystals* (Interscience, New York, 1968).
[8] G. Blasse, in *Luminescence of Inorganic Solids*, edited by B. DiBartolo (Plenum, New York, 1978), p. 175.
[9] J. H. Walker, R. D. Saunders, J. K. Jackson, and D. A. McSparron, *NBS Measurement Services: Spectral Irradiance Calibrations*, Nat. Bur. Stand. Spec. Pub. 250-20 (U.S. Govt. Printing Office, Washington, D.C., 1987).
[10] T. C. Larason, S. S. Bruce, and C. L. Cromer, J. Res. Natl. Inst. Stand. Technol. **101**, 133 (1996).
[11] L. H. Robins, E. N. Farabaugh, and A. Feldman, Phys. Rev. B **48**, 14 167 (1993).
[12] D. Curie, in *Optical Properties of Ions in Solids*, edited by B. DiBartolo (Plenum, New York, 1975), p. 71.
[13] R. Ramnirane and W. F. Sherman, Infrared Phys. **26**, 17 (1986).
[14] D. T. Brower and I. K. Lloyd, J. Mater. Res. **10**, 211 (1995).
[15] Y. Nakao, J. Phys. Soc. Jpn. **48**, 534 (1980).
[16] S. P. Keller, Phys. Rev. **111**, 1533 (1958).
[17] W. Lehmann, J. Lumin. **15**, 87 (1972).
[18] D. T. Brower and R. E. Revay, Proc. SPIE **1663**, 86 (1992).